JOURNAL OF MATERIALS SCIENCE **40** (2005) 295–308

Predicting fatigue S-N (stress-number of cycles to fail) behavior of reinforced plastics using fracture mechanics theory

M. G. WYZGOSKI, G. E. NOVAK
Delphi Research Labs, Delphi Corporation, 51786 Shelby Parkway, Shelby Township, MI 48315, USA
E-mail: michael.g.wyzgoski@delphi.com

The present study describes a model to predict fatigue S-N behavior, and thus fatigue life, of glass fiber reinforced thermoplastics by using a fracture mechanics approach. The model assumes the presence of an inherent initial flaw in the molded plastic parts and thus ignores crack initiation contributions. In this paper we describe how fatigue crack propagation rate data were obtained for the same three glass fiber reinforced plastics whose S-N behavior was previously described in detail. Using the measured constants from the crack growth data, and corresponding S-N data for uncracked specimens, the validity of the single initial flaw hypothesis was evaluated. From the analyzed results it is concluded that accurate S-N predictions are possible using this simple fracture mechanics model for some materials. The best results are obtained for glass filled polyamide, PA (nylon 66) and polycarbonate, PC; however, with polybutylene terephthalate, PBT, predictions were poor. It is also shown that S-N data for different glass fiber orientations can be predicted by combining the single flaw model with predicted fatigue crack propagation rate measurements. The latter are calculated from a generalized crack growth rate expression utilizing the strain energy release rate fracture mechanics parameter, which was previously described.

1. Introduction

Both fracture mechanics approaches and stress or strain versus lifetime curves have long been utilized to characterize fatigue failure of metals [1, 2]. In their seminal textbook Hertzberg and Manson described both approaches for fatigue of polymeric materials [3]. Strictly speaking, linear elastic fracture mechanics theory was not developed for inhomogeneous materials, however it has proven very useful for such materials. Reifsnider has summarized much of the work on composite materials, including short fiber reinforced thermoplastics [4]. Earlier studies in our laboratories have similarly demonstrated the value of using a fracture mechanics approach to characterize the fatigue behavior of glass fiber reinforced thermoplastics, both for reaction molded and injection molded materials [5, 6]. In particular, fatigue crack propagation rate measurements have been shown to provide an accelerated method of establishing the relative fatigue resistance of this class of materials, as well as their unreinforced counterparts [7]. Furthermore, the present authors have extended the application of this basic theory by showing that fatigue data for different fiber orientations collapse onto a single master curve if the crack propagation rate data are expressed in terms of strain energy release rate [6]. This relationship can be used to make predictions of material and processing effects on fatigue resistance. For example, the influence of fiber orientation, fiber type, and fiber concentration can be predicted from the crack propagation rate measurements on one composition given that moduli information are available or can be calculated. Others have found this relationship equally valuable for interpreting frequency effects for glass reinforced materials [8].

Although the fracture mechanics approach has proven very valuable for material comparisons and for assessing fatigue resistance in a relatively short time, plastic part designers are generally seeking the more traditional stress-lifetime or S-N type of data for a material. The latter lends itself to modern day stress analyses by finite element analysis and is certainly more easily understood and easier to implement into a plastic component lifetime prediction.

Recently, our attention has therefore been focused on the measurement of the fatigue resistance of uncracked specimens with this more traditional approach by measuring the number of cycles to fail, N, for injection molded samples at various initial stress levels, S. Thus, the generation of S-N data for three glass-reinforced plastics under a variety of loading and fiber orientation conditions has already been reported [9, 10]. Fatigue testing of uncracked specimens is unfortunately

very time consuming. For example, to generate a single S-N curve typically requires weeks to months of testing time with multiple specimens on relatively expensive servohydraulic testing equipment. On the other hand, the generation of a basic fatigue crack propagation rate curve can be obtained in a matter of hours with a single specimen. Experience with S-N testing made it clear that it would be highly desirable to be able to combine the advantage of the fracture mechanics test, namely high speed, with the advantage of the S-N test, namely the data are more useful for part design.

In the present study, and a companion paper to follow, we will demonstrate the extent to which this is feasible by using the accelerated fatigue crack propagation rate measurements and fracture mechanics theory to predict the corresponding S-N data for glass fiber reinforced thermoplastics. First, we will test the simple hypothesis that there exists an inherent initial flaw in the injection molded sample, which propagates under fatigue loading to complete rupture or failure. This assumes no contribution to fatigue lifetime from crack initiation. We will also provide additional data on the use of the strain energy release rate parameter, G, for representing the fatigue crack propagation rate data. The latter has been directly measured by monitoring compliance data and this will be compared with our previous method for calculating G from modulus and Poisson's ratio. The strain energy approach will be of critical value since in highly oriented samples it has been found that obtaining crack growth rate data in certain orientations is problematical as will be discussed in this paper. Furthermore we will describe a more detailed method for precracking the fracture mechanics samples to improve the reproducibility of the results.

2. Theory

Fracture mechanics theory and its application to plastics have been well described in the literature including several texts [11–14]. Stress is defined in the usual sense for S-N testing however for the fracture mechanics specimens the stress is replaced with the stress intensity factor term, defined as:

$$K = Y\sigma\sqrt{a} \tag{1}$$

where K = Stress Intensity Factor, Y = Geometry Factor, σ = Stress, and a = Crack Length.

Y is a dimensionless factor, which can be found for specific geometries in handbooks [15]. Thus K has units of stress times a length to the half power. In a typical single cycle test to failure, the conventional tensile test would determine a value for breaking stress whereas the fracture mechanics equivalent would be to determine a value of K at which breaking or fracture occurs. The latter is referred to as K_{1c}, the fracture toughness of the material. An ASTM Standard for fracture toughness determinations for plastics has been written [16] following earlier efforts by the European Structural Integrity Society, ESIS [14]. For fatigue testing, loads below that needed to initiate fracture are employed, while one still uses the above expression to define the crack tip stress intensity factor. As with metals, the growth rate of a fatigue crack of length a is generally well described by the stress intensity factor using the Paris equation [3]:

$$\frac{\mathrm{d}a}{\mathrm{d}N} = A\Delta K^{\mathrm{m}} \tag{2}$$

where a = Crack Length, N = Number of Fatigue Loading Cycles, A = Intercept of a log-log plot of $\mathrm{d}a/\mathrm{d}N$ vs. ΔK, and m = Slope of log-log plot of $\mathrm{d}a/\mathrm{d}N$ vs. ΔK.

For the glass fiber reinforced materials we have previously shown that, although fiber orientation strongly influences crack growth rates, the data collapse onto a single curve when expressed in terms of ΔG, the strain energy release rate [6, 18]. For these studies G has been calculated as:

$$G = (1 - \nu^2) \times \left[\frac{K^2}{E}\right] \tag{3}$$

where ν = Poisson's ratio and E = Modulus.

Although in some cases the Poisson's term was ignored. Using this expression one need only have crack growth rate data for one glass fiber orientation along with the corresponding mechanical constants to calculate the $\mathrm{d}a/\mathrm{d}N$ versus ΔG master curve. The $\mathrm{d}a/\mathrm{d}N$ versus ΔK relationship can then be calculated for all other fiber orientations. Because this is a critical step in ultimately attempting to predict fatigue life for the different orientations, it was deemed important to evaluate other approaches to determine G. Specifically, G can be directly measured during the fatigue crack propagation rate experiment. Two different methods were employed and detailed results were presented earlier [19]. First, the values of G at maximum and minimum loads were independently assessed from the area under the load-displacement curve by generally following the procedures outlined in the ASTM Standard for G_{1c} determination [16]. This approach utilizes the relationship:

$$G = \frac{U}{(BW\varphi)} \tag{4}$$

where U = energy (area under the curve), B = thickness, and ϕ = calibration constant for the compact tension geometry.

A second method for directly determining G was investigated since the fiber reinforced materials are anisotropic and the area method above, particularly the constant ϕ, is strictly speaking valid only for isotropic materials. The second method is based upon measuring compliance during the fatigue crack growth rate experiment and using the expression [12, 13]:

$$G = \left(\frac{P^2}{2B}\right) \times \left(\frac{\mathrm{d}C}{\mathrm{d}a}\right) \tag{5}$$

where P = load, B = thickness, C = sample compliance, and a = crack length.

What is required is a determination of the compliance-crack length relationship in order to subsequently calculate the derivative of this curve. Obviously the two methods for direct determination of ΔG, if successful, offer the advantage that independent modulus and Poisson's ratio measurements would not be needed.

Once we have selected a method to obtain fatigue crack growth rate data, such data can then be related to the corresponding S-N results for the same material by integrating the Paris equation and substituting the expression for K to give [3]:

$$N_{\mathrm{f}} = \frac{2}{(m-2)AY^{\mathrm{m}}(\Delta\sigma)^{\mathrm{m}}}\left(\frac{1}{a_0^{\frac{(\mathrm{m}-2)}{2}}} - \frac{1}{a_{\mathrm{f}}^{\frac{(m-2)}{2}}}\right) \quad (6)$$

Here N_{f} is the final or total number of cycles to fail. To employ this equation for calculating fatigue lifetime, we can use the m and A values which are obtained from the crack propagation experiment, and select a value of Y based upon the specimen geometry; but we must also know the initial and final crack or flaw sizes. The latter can be set equal to the sample thickness or estimated from fracture toughness values. However, generally the initial flaw size is unknown. On the other hand, if S-N data are available, then we can calculate the initial flaw size by simply using the S-N data to provide pairs of N_{f} and $\Delta\sigma$ along with the known A, m, and Y values. Thus it is possible by rearranging the above equation to determine values of a_0, or initial crack lengths, which presumably represent inherent flaws in the material. The expression for the initial crack or flaw size is:

$$a_{\mathrm{o}} = \left[\frac{1}{\frac{N_{\mathrm{f}}(m-2)AY^{\mathrm{m}}\Delta\sigma}{2} + \frac{1}{a_{\mathrm{f}}^{(\mathrm{m}-2)/2}}}\right]^{2/(m-2)} \quad (7)$$

As just mentioned, the final flaw size can be set equal to the thickness of the sample, however, it was determined through calculations that this term can be set equal to infinity without significantly changing the resultant value of a_0. One difficulty in making this type of calculation is that the selection of a value for Y is somewhat arbitrary. Although Y can be clearly defined for a given type of loading, specimen and flaw geometry [15], the latter is unknown in general and therefore requires some assumptions. Moreover, strictly speaking, Y is known to be a function of crack length, which means that a more complicated iterative mathematical solution is required. In this first study the value for Y was fixed at 1.17, which is based upon a semicircular surface flaw [15]. Our calculated values of flaw size will be dependent on this choice of Y; however, our focus here was on the predictability of S-N data, not on the absolute value of the flaw size. For this purpose, one need only be consistent in the choice of Y. A test of the validity of the fracture mechanics approach is then to examine the initial flaw size as a function of stress level. A constant value should be obtained if the fracture mechanics approach is valid.

3. Experimental

3.1. Materials

The glass fiber filled materials employed included the following: thirty three percent by weight glass filled nylon 66 polyamide, PA, DuPont's Zytel 70G33L; thirty percent by weight glass filled polybutylene terephthalate, PBT, General Electric's Valox 420; and thirty percent by weight glass filled polycarbonate. For the PBT, two different batches of material were used. An initial batch was found to contain shorter glass fiber lengths and was considered not representative of the commercial material. It was designated PBT Batch A and was used for preliminary fatigue crack growth rate measurements which helped establish a uniform procedure. A second PBT batch, termed PBT Batch B, had longer fiber lengths and was deemed more representative or "typical" in terms of mechanical properties. For consistency the PBT Batch B was utilized for both the S-N measurements and the fatigue crack growth rate data for flaw size determinations.

3.2. Specimen preparation

Three different plaque geometries were utilized in this study. Determinations of G directly were first performed using compact tension specimens cut from a $3.2 \times 50.8 \times 203.2$ mm end-gated plaque of the PA material as described previously [19]. Subsequently all other measurements were performed with somewhat larger plaques to permit cutting both tensile specimens and compact tension specimens. For preliminary fatigue crack growth rate measurements, the PBT Batch A was injection molded into a $3.2 \times 76.2 \times 279.6$ mm end gated plaque. Compact tension specimens were cut from the center section of this plaque in either the Flow or Xflow direction. Subsequently an injection molded ribbed plaque was utilized for cutting specimens for all fatigue crack propagation rate measurements. This same ribbed plaque had been selected to prepare all specimens for S-N data generation as was previously reported [9, 10]. For the present study, the fatigue cracks were caused to grow in the same region of the plaques where cracks had initiated during the S-N measurements. The geometry of this plaque is shown in Fig. 1

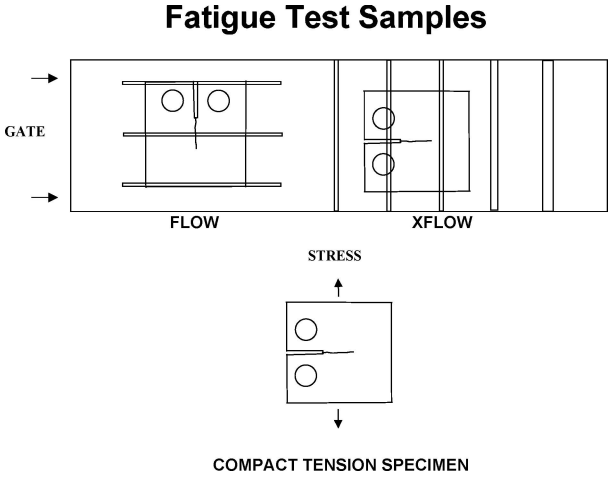

Figure 1 Geometry of ribbed plaque showing location and shape of compact tension specimens for Flow and Xflow orientations.

along with schematic views of the Flow and Xflow oriented compact tension specimens. A detailed investigation of the fiber orientation for the ribbed plaque has also been reported by Tucker, and O'Gara [17]. They described a typical shell/core structure with a high degree of fiber alignment along the flow direction in the outer shell regions and a narrow core section in the center of the thickness. Thus the measurements reported here for this injection molded ribbed plaque represent the near extreme expected in terms of anisotropy for the materials.

3.3. Tensile property determinations

Both Flow (stress axis parallel to melt flow direction during injection molding) and Xflow (stress axis transverse to melt flow direction) tensile properties were determined by machining the smaller ASTM Type V dogbone shaped specimens from the ribbed plaques. Specimens were tested at a crosshead speed of 5.1 mm/min which corresponds to a strain rate of 0.0016/s. A strain gauge having a length of 7.6 mm was employed and modulus determinations were made over a strain range of 0.1 to 0.5%. For Poisson's ratio measurements, a separate biaxial strain gauge was employed which required a 25.4 mm gauge length. For these measurements straight strips, 12.7 × 76.2 mm were used and calculations followed the ASTM E-132 standard.

3.4. Fatigue crack propagation rate measurements

The detailed procedure for measuring fatigue crack growth rates has been previously published along with a description of the compact tension specimen geometry for the 3.2 × 50.8 × 203.2 mm plaque [6, 7]. For consistency with the earlier results, this plaque was utilized initially for comparison of the calculated versus measured strain energy release rates for the PA material. As mentioned earlier, in order to express the data both in terms of the oscillating stress intensity factor, ΔK, and strain energy release rate, ΔG, an extensometer was employed on the grips of the compact tension specimen. This allowed a direct determination of ΔG from both the area and compliance approaches for comparison with calculated ΔG values from the independently measured moduli and Poisson's ratios. Subsequently, the ribbed plaque geometry was employed for fatigue crack propagation rate measurements since it had previously been utilized for extensive S-N measurements for all three materials. The compact tension geometry was identical to that used previously and Fig. 1 shows the layout of the compact tension specimens in the ribbed plaque. Note that the local area used for fatigue crack growth measurements was selected away from the regions where ribs were milled off, although the overall compact tension specimen initially included these regions. Fatigue crack propagation rate measurements were performed at a frequency of 0.5 Hz and an R-ratio of 0.1 (ratio of minimum to maximum load). The lower frequency was selected to avoid any possibility of hysteretic heating contributions which would be localized at the crack tip. In the absence of hysteretic heating no effect of frequency is observed for these materials at room temperature.

TABLE I Tensile properties of materials

	Tensile modulus (GPa)		Tensile strength (MPa)		Poisson's ratio	
Material	Flow	XFlow	Flow	XFlow	Flow	XFlow
PA	9.4	5.4	182	100	0.43	0.28
PBT	8.2	4.3	92	55	0.46	0.29
PC	7.4	4.0	101	66	0.48	0.28

4. Results

4.1. Tensile properties

The strength, modulus and Poisson's ratio for the three glass fiber filled materials are given in Table I for both the Flow and Xflow directions for specimens cut from the ribbed plaques. In general the data demonstrate the high degree of anisotropy expected from the fiber orientation mentioned earlier [17].

4.2. Fatigue crack propagation rate measurements

4.2.1. Initial strain energy determinations

Using the 3.2 × 50.8 × 203 mm end gated plaque, Fig. 2 shows the significant effect of fiber orientation on fatigue crack growth rates for PA when plotted in the usual manner versus stress intensity factor, or ΔK. Considering the log scales, the effect of fiber orientation is very strong as expected. Fig. 3 indicates the collapsing of these data onto a single line when expressed on a calculated ΔG basis. This duplicates our earlier results [6]. However, Fig. 3 also shows that the directly measured ΔG data for the flow direction using the compliance method (see Flow Comp in Fig. 3) does not fall

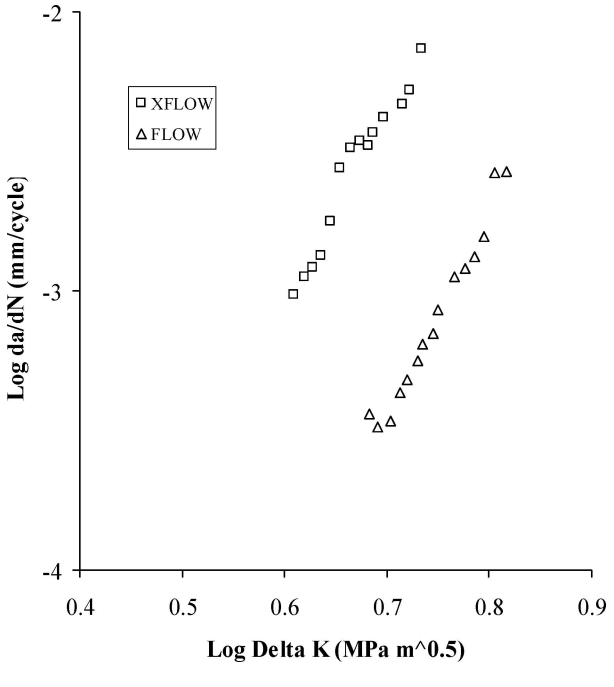

Figure 2 Fatigue crack propagation rate data for PA in the 3.2 × 50.8 × 200.3 mm plaque for Flow and Xflow orientations.

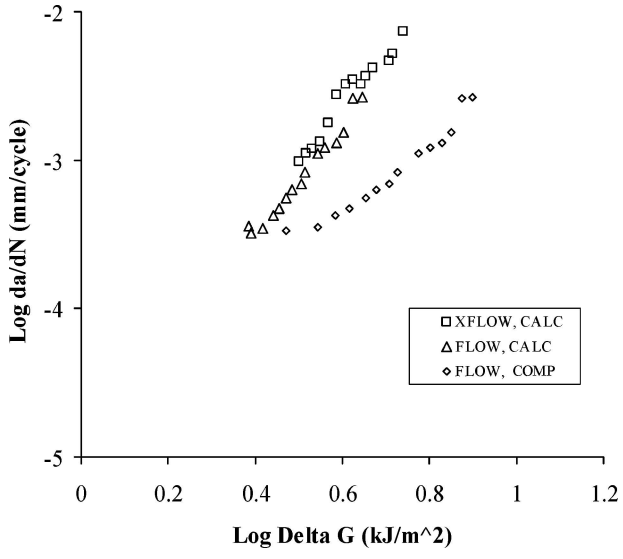

Figure 3 Fatigue crack growth rate data from Fig. 2 replotted in terms of calculated ΔG. The directly measured ΔG in the Flow direction using the compliance method is shown for comparison.

in the same vicinity. The directly measured ΔG results determined using the area method were similar to the compliance data for Flow direction samples. This discrepancy between calculated versus directly measured ΔG values is limited to the flow direction samples. As shown in Fig. 4, the Xflow direction specimens provide very similar results for the crack growth in terms of ΔG for all methods of calculating or directly measuring the strain energy release rate. Possible explanations for the differences for the Flow direction specimens will be discussed in a later section. However, these results indicate that calculating the strain energy values from moduli and Poisson's ratios would seem to be the only way to obtain a single master curve for each material.

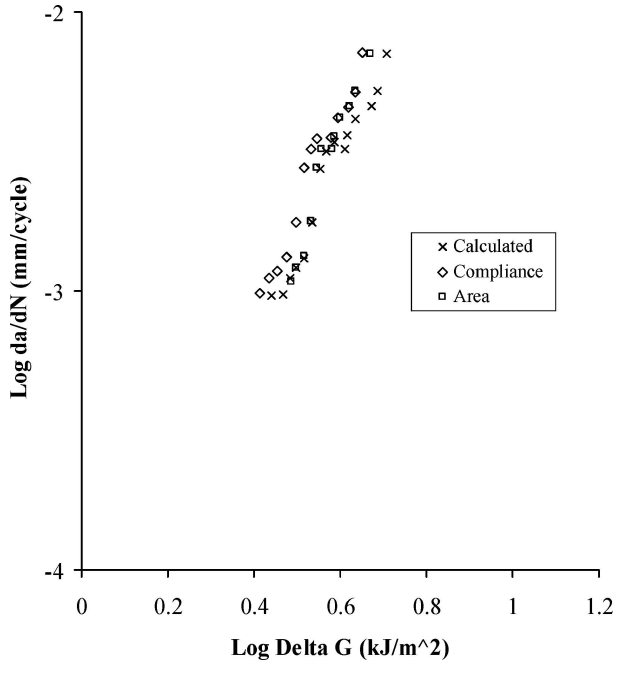

Figure 4 Comparison of calculated and directly measured ΔG for PA in the Xflow orientation.

4.2.2. Ribbed plaque-PA

The crack growth results obtained for the slightly thinner PA ribbed plaque were similar in character to the extensive data obtained earlier with the 3.2 × 50.8 × 203 mm end gated plaque [6] with two significant exceptions. For the Xflow sample, fatigue crack growth rate measurements were obtained with ease following our previous procedure. Fig. 5 shows the data expressed in terms of both ΔK and the directly measured ΔG. The first exception mentioned above is that for the ribbed plaques it was not possible to obtain colinear fatigue crack propagation for the Flow specimen (with the crack oriented perpendicular to the predominant fiber orientation). This was not only true for the PA, but also was the case for PBT-Batch B and the PC materials. Although stable fatigue crack growth did generally occur, in most cases the crack path would eventually turn upward (or downward) to follow the preferred fiber orientation direction making the calculation of ΔK invalid. Although it was possible to obtain enough limited

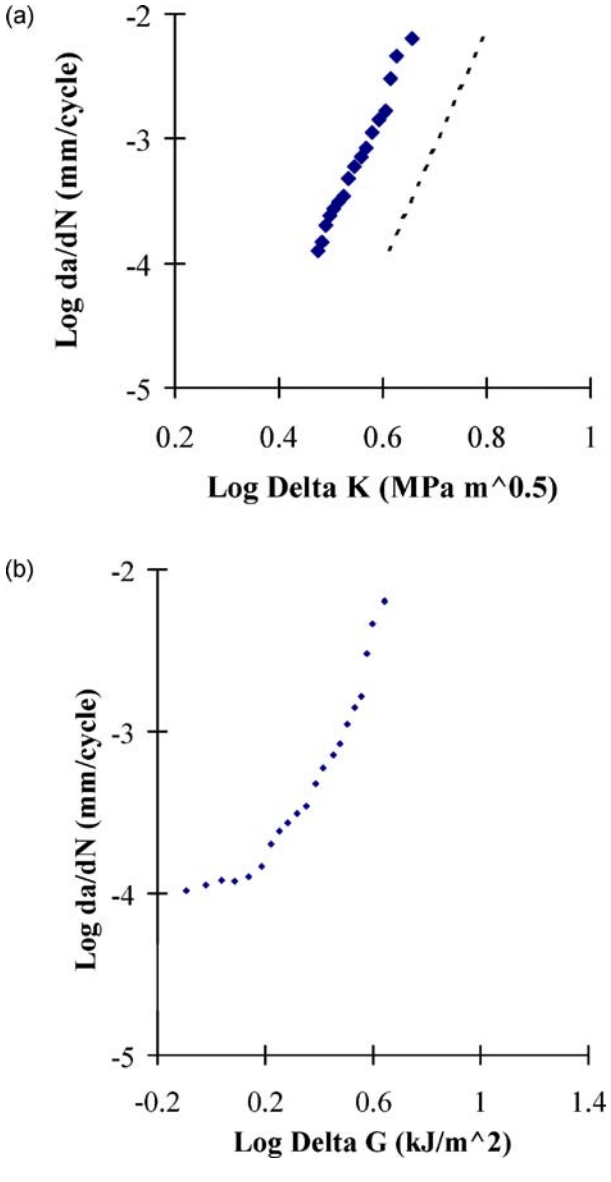

Figure 5 (a) Fatigue crack propagation rate versus stress intensity factor for PA in the Xflow orientation. Dashed line represents calculated values for Flow orientation. (b) Same data as in (a) replotted versus strain energy release rate.

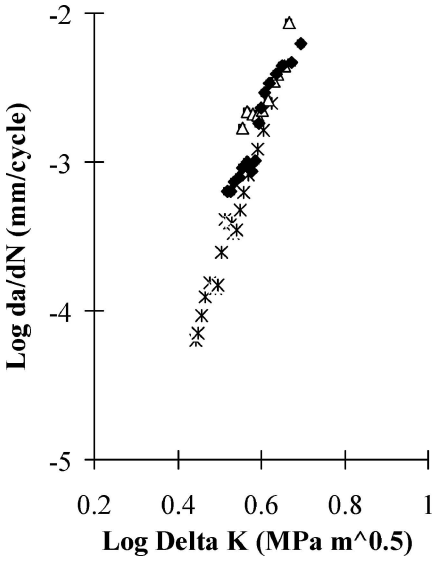

Figure 6 Fatigue crack propagation rate versus stress intensity factor for PBT in the Xflow orientation. Symbols represent specimens started at different load levels, i.e., different initial ΔK values.

data to insure the growth rates were of the expected magnitude for the Flow direction orientation, a complete data set for determining Paris equation constants could not be obtained. This had never been observed in the slightly thicker 3.2 × 50.8 × 203 mm plaques and we tentatively associate this with the higher orientation and/or thinner core regions which are observed in the ribbed palque.

Since the intent of this study was to predict the S-N data which was generated from the ribbed plaque for both flow and crossflow orientations, it was decided that the needed fatigue crack propagation rate data for the flow direction would be predicted using the strain energy release rate master curve approach based upon the calculated values as mentioned above [6]. This predicted flow direction da/dN behavior for PA is shown as the dashed line in Fig. 5.

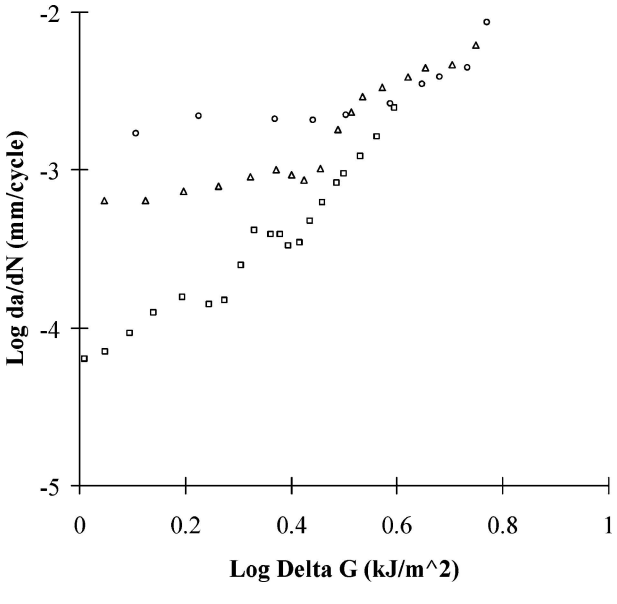

Figure 7 Fatigue crack propagation rate versus directly measured strain energy release rate for PBT in the Xflow orientation (same experiments as in Fig. 6).

An additional revelation from using the ribbed plaque, not previously seen in the other plaque, is the fact that the initial fatigue crack growth data often showed a hesitation or decreased slope at the start of the crack growth experiment. In terms of ΔK , the hesitation is often not pronounced, and can be interpreted as data scatter which is generally not included in the plots. However, the initial slope change in the crack growth rate was observed to be accentuated and well behaved when the results are expressed in terms of the directly measured ΔG, as shown in Fig. 5b. Repeated measurements showed that this behavior was very reproducible Again, since the present study was focused upon curve fitting the measured data sets to obtain accurate slopes for extrapolation to lower ΔK, it was important to understand any deviant or transient data at the low ΔK levels at the start of the test. A similar slope change had

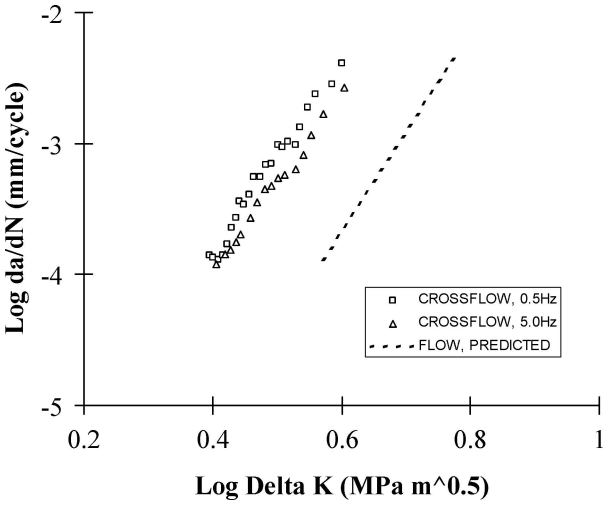

Figure 8 Fatigue crack propagation rate versus stress intensity factor for PBT from ribbed plaque showing slight effect of frequency for Xflow orientation. Dashed line is predicted result for Flow orientation.

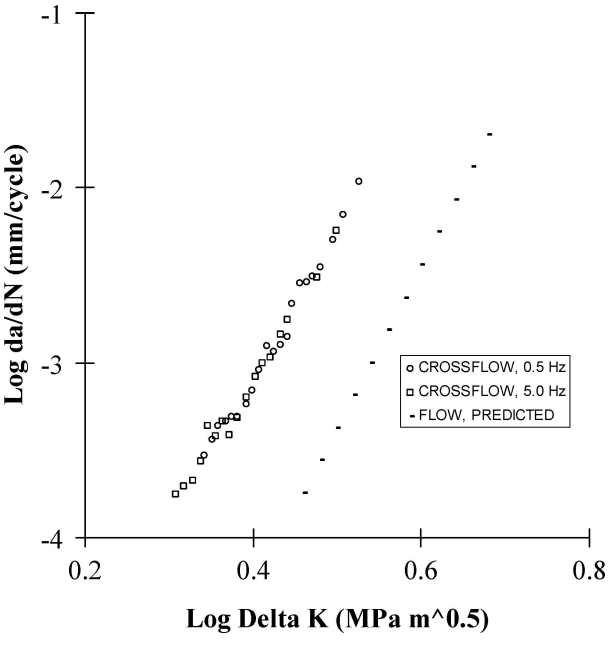

Figure 9 Fatigue crack propagation rate versus stress intensity factor for PC showing no effect of frequency for Xflow orientation. Dashed line is predicted result for the flow orientation.

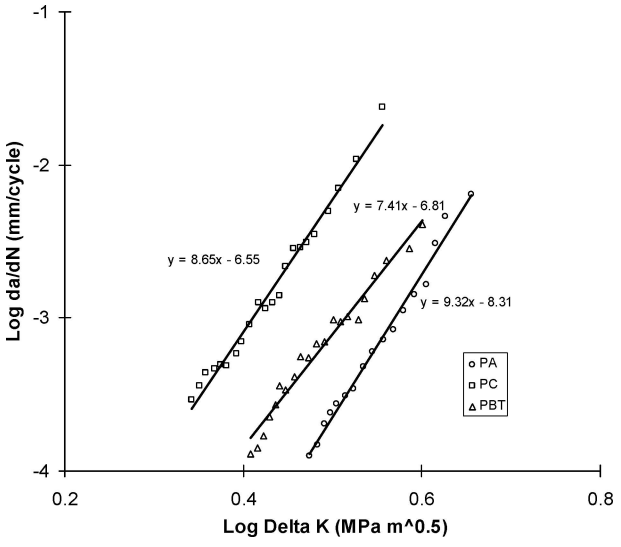

Figure 10 Fatigue crack propagation rate versus stress intensity factor for all three materials showing linear fit of data for determining Paris Equation constants.

been noted in the fatigue crack growth data for PBT specimens molded in the ribbed plaques as well as in a 3.2 mm thick plaque without ribs. The latter was chosen for a more detailed study since for PBT there were no concerns or issues with regard to moisture content.

TABLE II Fatigue crack growth parameters

Material	Stress	Orientation	a_o (μm)	A (m/cycle)	m
PA	Tensile	Flow	511	2.6 E-13	9.32
	Tensile	XFlow	758	4.9 E-12	9.32
	Flex	Flow	188	2.6 E-13	9.32
	Flex	XFlow	386	4.9 E-12	9.32
PBT	Tensile	Flow	1402	7.92 E-12	7.41
	Tensile	XFlow	1192	1.53 E-10	7.41
	Flex	Flow	216	7.92 E-12	7.41
	Flex	XFlow	385	1.53 E-10	7.41
PC	Tensile	Flow	1324	9.27 E-12	8.65
	Tensile	XFlow	1899	2.82 E-10	8.65
	Flex	Flow	431	9.27 E-12	8.65
	Flex	XFlow	411	2.82 E-10	8.65

4.2.3. PBT- Batch A

Preliminary measurements for PBT were made using the 3.2 × 76.2 × 203 mm plaque and using the first lot of Valox 420 material which again we term PBT-Batch A. Fig. 6 shows the results of a systematic analysis of these PBT specimens which were fatigued under identical conditions except the load was varied to achieve a different initial stress intensity level. The curves at different ΔK roughly overlap, as required by fracture mechanics theory. However, a closer look indicates that the initial data in each data set is slightly

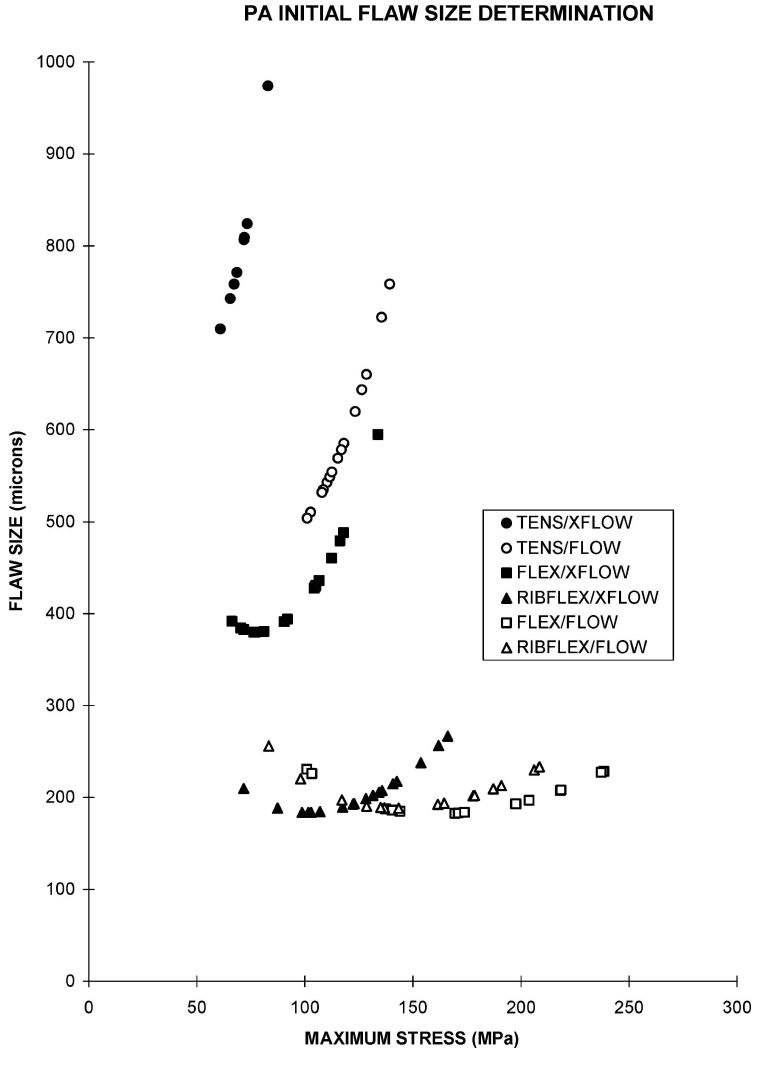

Figure 11 Initial flaw sizes for PA material calculated from various S-N datasets as indicated. See Reference 9 for details on S-N data.

deviant, while generally the data for each test does in fact overlap at the higher ΔK levels. The corresponding da/dN-ΔG plots for the same fatigue crack growth rate data where ΔG was determined using the compliance method are given in Fig. 7. The ΔG results more clearly reveal two regimes of behavior with vastly different slopes for the crack growth rate data. The deviation, or initial transient response, is highly load dependent and does not simply overlap as it should according to fracture mechanics theory.

The peculiar transition described above would appear to invalidate any attempt to fit the entire crack propagation rate data set with a straight line, as required to determine the Paris equation constants. However, it is also clear that once these transient data are removed, the data sets do in fact collapse onto a single curve as required by fracture mechanics theory. The use of the directly measured ΔG data provides one possible way to perform data editing. As an alternative, a testing procedural change was found to minimize the initial transient response. Specifically the compact tension specimens were precracked not only with a series of saw and razor cuts as before, but also by initiating a fatigue precrack. The latter was generated at a higher load and at a higher frequency (5.0 Hz) until the fatigue portion of the precrack length reached approximately 5 mm. This was not an arbitrary choice, but rather was based upon measuring the crack length at the transition point in the fatigue crack propagation rate data sets shown in the above figures. This procedure was subsequently used for all of the fatigue crack propagation rate data taken for the ribbed plaques.

4.2.4. PBT-Batch B

Ribbed plaques were molded for both PBT batches in order to compare their fatigue behavior. As expected, owing to the decreased average fiber length mentioned earlier, Batch A exhibited somewhat accelerated fatigue crack growth rates at all ΔK levels. Since fatigue S-N data were only generated previously for the Batch B, we focus here on those results, which are shown in Fig. 8. The ΔK and ΔG plots for this precracked specimen were well behaved with little scatter.

However, a slight effect of frequency was noted in comparing the data at 0.5 and 5.0 Hz. A frequency effect is not reported for PBT in the literature and we

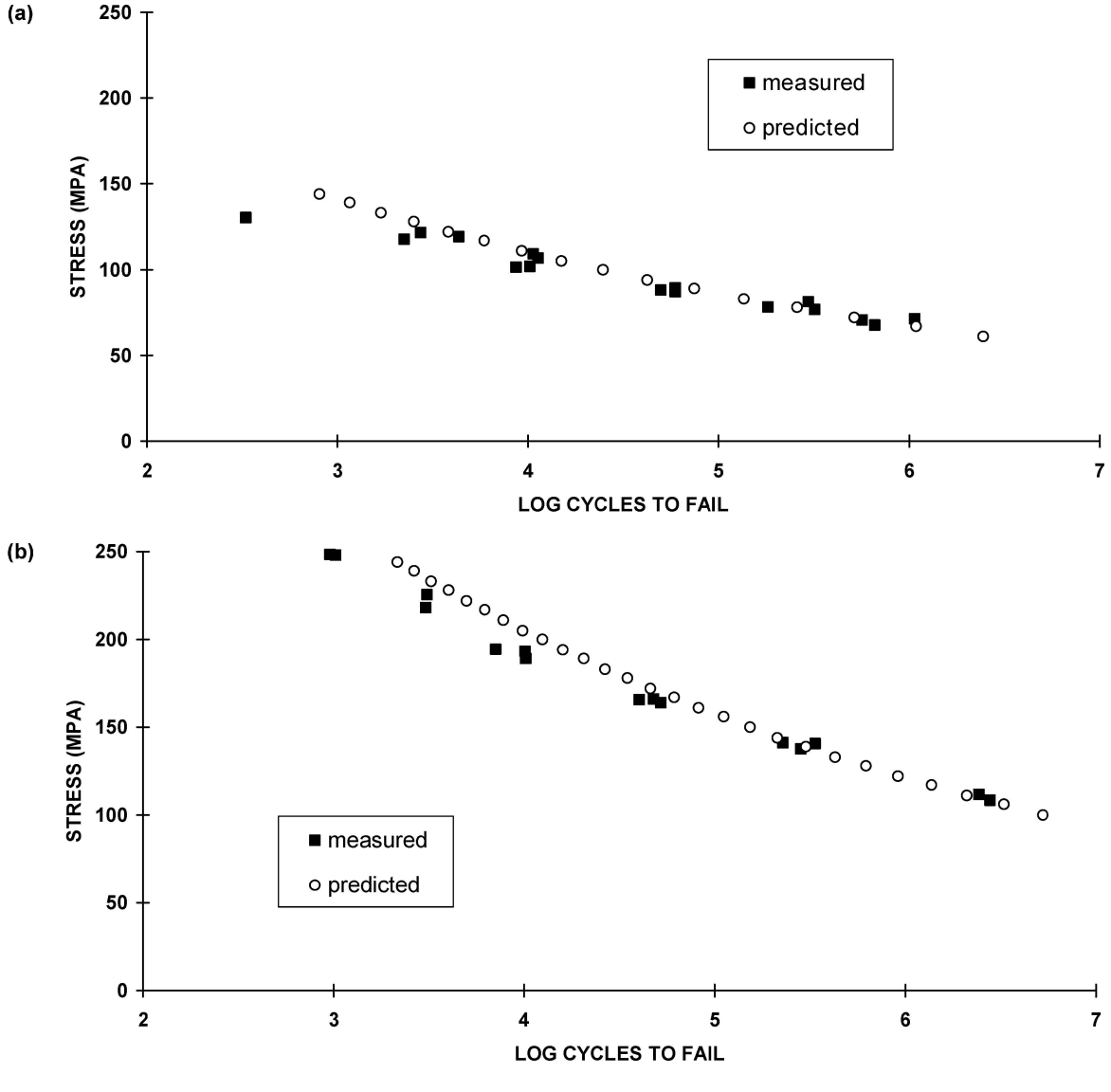

Figure 12 Comparison of predicted and measured S-N data for PA in the flexural fatigue test for the (a) Xflow and (b) Flow direction specimens.

tentatively suspect a contribution from creep at the lower frequency. For consistency with the other materials the 0.5 Hz data were still used in flaw size determinations. Also shown in Fig. 8 are the predicted results for the flow orientation since once again colinear crack growth rate data could not be obtained for this orientation in this thinner plaque. As mentioned earlier, the predicted flow direction results are based upon the calculated ΔG master curve for this material.

4.2.5. PC

The effect of frequency on fatigue crack growth for the glass reinforced PC material in the crossflow orientation was not found in the literature and it was felt necessary to confirm the lack of a frequency dependence. Fig. 9 shows the crack growth rate data at both 5.0 and 0.5 Hz for the crossflow orientation. There clearly is no frequency dependence exhibited in these data. Fig. 9 also shows the predicted flow direction data for the PC which is derived from the calculated strain energy release rate values. The fatigue crack propagation rates for the PC are much more rapid than observed for either PA or PBT which is attributed to the amorphous nature of this polymer.

4.3. Paris equation constants

From the prior figures in this paper it is apparent that straight lines can be fit to the da/dN-ΔK data sets to provide values of A and m. This is further demonstrated in Fig. 10 where the crossflow data for each of the three materials is replotted and the corresponding Paris equation line is drawn through the data. Table II lists the A and m values derived from the curve fitting for the various materials.

4.4. Flaw size determinations

For any given pair of S-N values, or σ-N_f in the terminology of the equation given earlier, one can calculate the initial flaw size by inputting the corresponding A and m values for the material in the appropriate fiber orientation (flow vs. crossflow). For PA, Fig. 11 shows the calculated flaw sizes for the entire set of S-N data previously published [9, 10] for the ribbed plaque. The terminology simply refers to whether a tensile bar, a

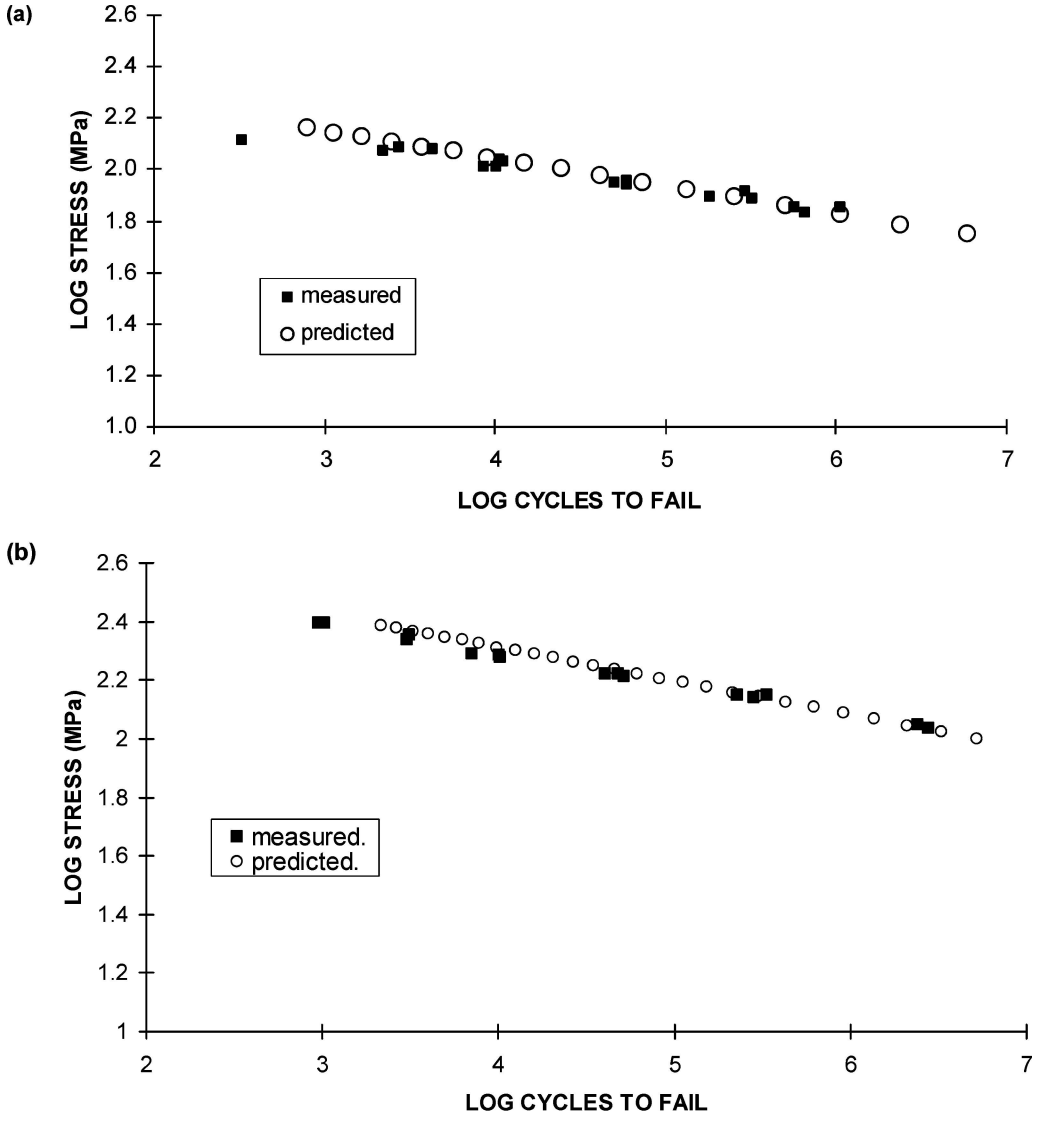

Figure 13 Comparison of predicted and measured S-N data for PA in the flexural fatigue test replotted on a log-log scale for the (a) Xflow and (b) Flow direction specimens.

flat section, or a rib section was fatigued and in what orientation. Note that in some cases the flaw size is a strong function of stress level, whereas for other S-N data a region of relative stress independence is apparent. The latter is implicit in the fracture mechanics theory applied in this work. In particular it is important that the flaw size appears independent of stress in the low stress region where fatigue life prediction is of most practical significance. This is more critical for the flexure data than for the tensile loading conditions. Possible reasons for this will be the subject of a future publication.

From the curves for the flexural fatigue of the flat samples, where the flaw size appears constant at various stress levels, the average initial flaw sizes for the PA are determined to be 188μ for the flow direction and 386μ for the crossflow direction. The fact that the flaw size is dependent upon orientation is perhaps not surprising for this highly anisotropic material. A physical interpretation of the flaw size is not the intent of this publication. Table II summarizes the average flaw sizes along with the values for A and m from the crack growth rate data used in the determination of a_0.

To see how well the assumption of a constant flaw size allows us to "fit" the S-N data, the value for a_0 is substituted back into the equation for N_f at the corresponding stress levels used in the original S-N test. Fig. 12 shows the calculated versus measured S-N curves for PA for the two different orientations. An excellent fit or prediction is obtained even though for the crossflow case the flaw size is obviously not constant. In addition, it is interesting to note that the prediction for the flow direction actually represents a double prediction since it was first necessary to predict the needed crack growth rate data. This makes the observed result even more impressive.

The predicted curves in Fig. 12 are observed to be nonlinear on a semilog plot. A review of the equation used to derive these predictions indicates that the S-N relationship should be nonlinear on this type of plot, but should in fact be linear on a log-log plot. Fig. 13 shows the corresponding log-log plots and the measured data. A straight line fit to the data on a log-log plot appears very viable. This is also valuable in extrapolating the results to longer times. In the case of the crossflow direction, it is seen that the prediction would in fact

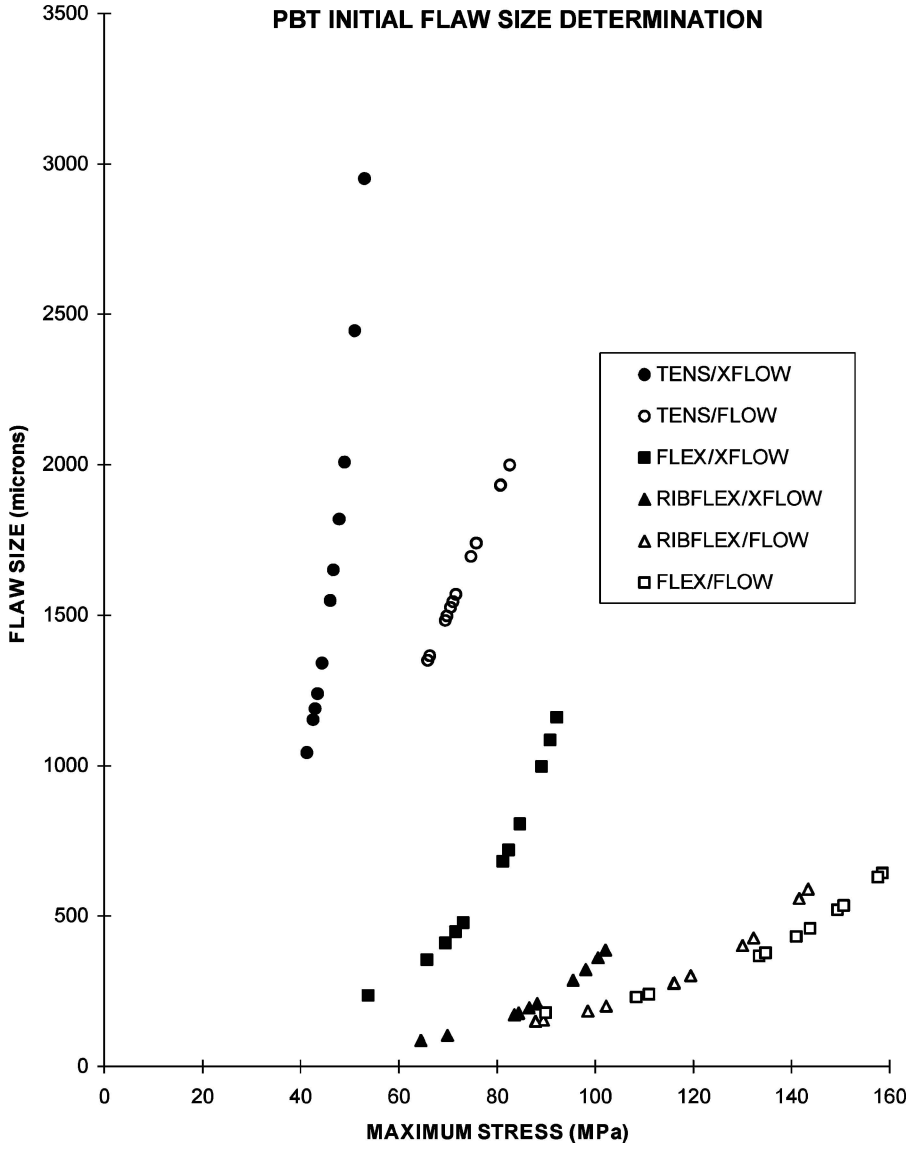

Figure 14 Initial flaw sizes for PBT material calculated from various S-N datasets as indicated. See Reference 9 for details on S-N data.

underestimate the fatigue life at longer times (ten or one hundred million cycles). Although indicating an inaccurate prediction, such a conservative estimate may be desirable for design purposes. For the flow direction, the predicted and experimental results match well at all stress levels and corresponding lifetimes. Following the literature, semilog plots are used subsequently for S-N plots.

For the PBT material the flaw sizes were much more dependent upon stress level at all values of stress. The plots in Fig. 14 appear similar to the PA flaw size plots; however the scale is greatly increased. Also it can be seen that for the PBT Flex/Xflow case the flaw size does not ever reach a constant value at lower stress levels. Thus the analysis did not provide a true constant flaw size. A minimum value was estimated by averaging the lower stress levels. Table II lists the estimated flaw sizes and Fig. 15 shows the predicted S-N behavior versus the measured results. The fit is obviously not good for either orientation. Possible explanations for this are given in the discussion that follows.

For PC the calculated flaw sizes were also highly stress dependent, however, the behavior differed from the PA and PBT. Fig. 16 shows that for the crossflow case at the lower stress levels the flaw size actually increased very dramatically. In fact the values are unrealistic as they are comparable to the sample thickness (2.5 mm). For the flow orientation, especially at the higher stress levels, the flaw size is surprisingly nearly constant. This suggests a change in the fatigue fracture mechanism compared to the crossflow orientation, particularly at the lower stress levels. The results for the crossflow orientation indicate that the observed fatigue failures in the S-N test are occurring more rapidly than expected based upon the measured fatigue crack growth rates. This is seen in Fig. 17 where the predicted and measured S-N curves are compared. The fit is poor for the crossflow orientation but is much better in the flow direction. This reasonably good fit for the flow direction is even more surprising since the flow crack growth rate data were in fact predicted from the crossflow measurements using the strain energy model.

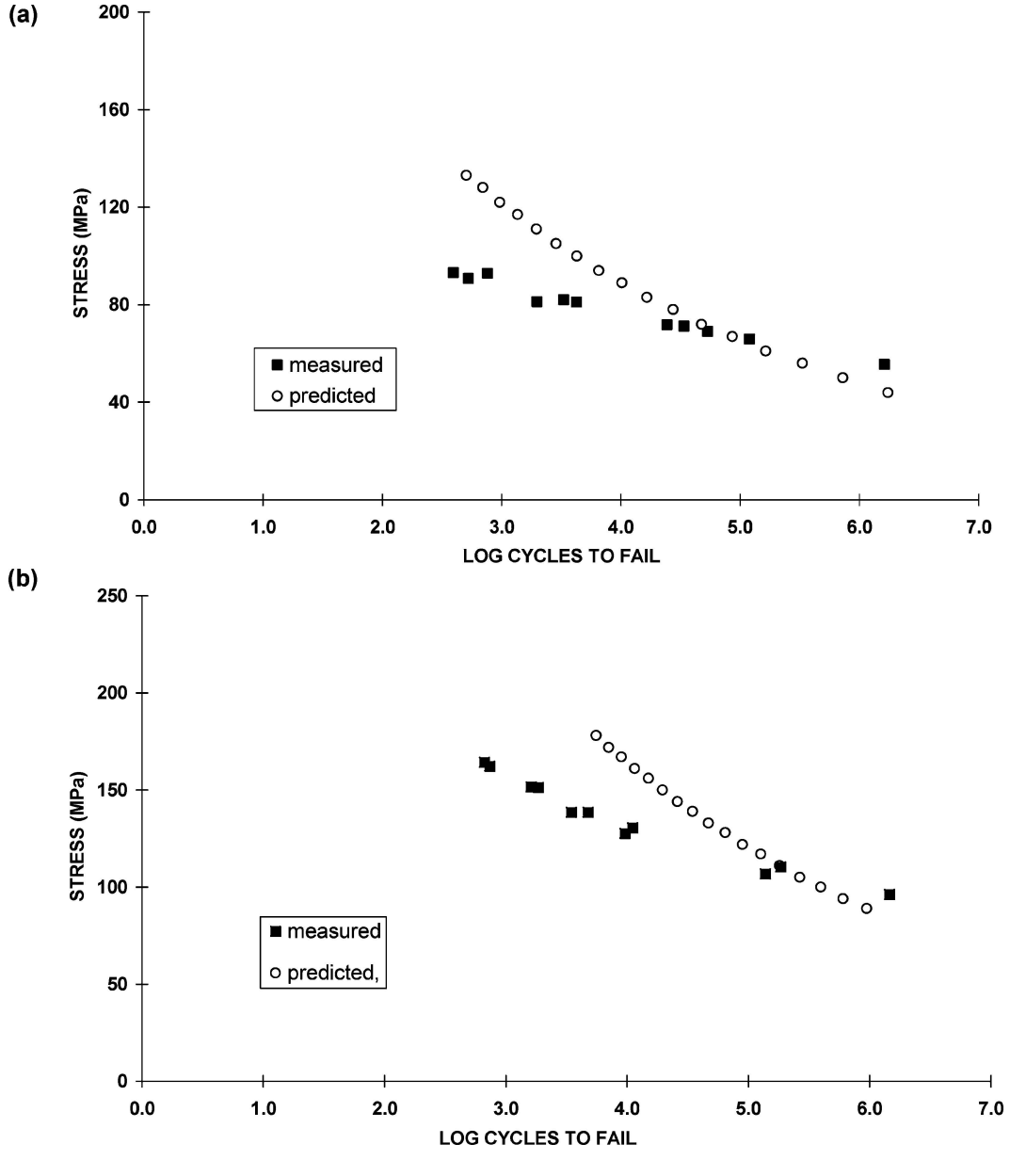

Figure 15 Comparison of predicted and measured S-N data for PBT in the flexural fatigue test for the (a) Xflow and (b) Flow direction specimens.

5. Discussion

5.1. Measurements of ΔG

The direct measurement of ΔG during the fatigue test was intended to provide a more accurate method for ultimately obtaining the master curve which previously had been calculated using moduli and Poisson's ratios for different fiber orientations. The lack of agreement for the measured and calculated values for the Flow direction was unexpected, and, is even more surprising given the agreement in the Xflow direction. The latter indicates the basic measurement approach is correct, especially considering that the compliance and area methods gave good agreement. Our explanation for the deviant results in the Flow direction is tentatively associated with the tortuous path of the fatigue crack for this orientation compared to the more colinear crack growth in the Xflow direction. This in turn relates to the fatigue crack growth mechanism, which, as reported earlier, involves the crack moving around fibers and fiber bundles rather than fiber fracture. While the more jagged crack profile for Flow direction specimens is very evident in the video observations used for crack growth measurements, a quantitative measure of the crack surface area for Flow versus Xflow orientations is more difficult. Also, the manner in which the fatigue crack growth rate is measured with our video system only reflects the crack advance orthogonal to the imposed stress. We therefore tentatively associate the higher directly measured ΔG with the increased surface area generated for fatigue fracture perpendicular to the dominant fiber orientation direction

5.2. Predicting S-N behavior

The mathematical model for predicting S-N behavior is straightforward once an initial flaw or initial crack length is known for the material. The results of this study demonstrate that one can obtain initial flaw sizes by first obtaining the required crack growth rate data along with a corresponding S-N curve. If a reasonably constant flaw size is observed at all stress levels, as it was for the PA, then this value should be treated as a material constant and it can be used to calculate a variety of S-N data. For any similar fiber orientation and mode of stressing one should be able to accurately calculate the S-N curve. For example, for the rib geometry the

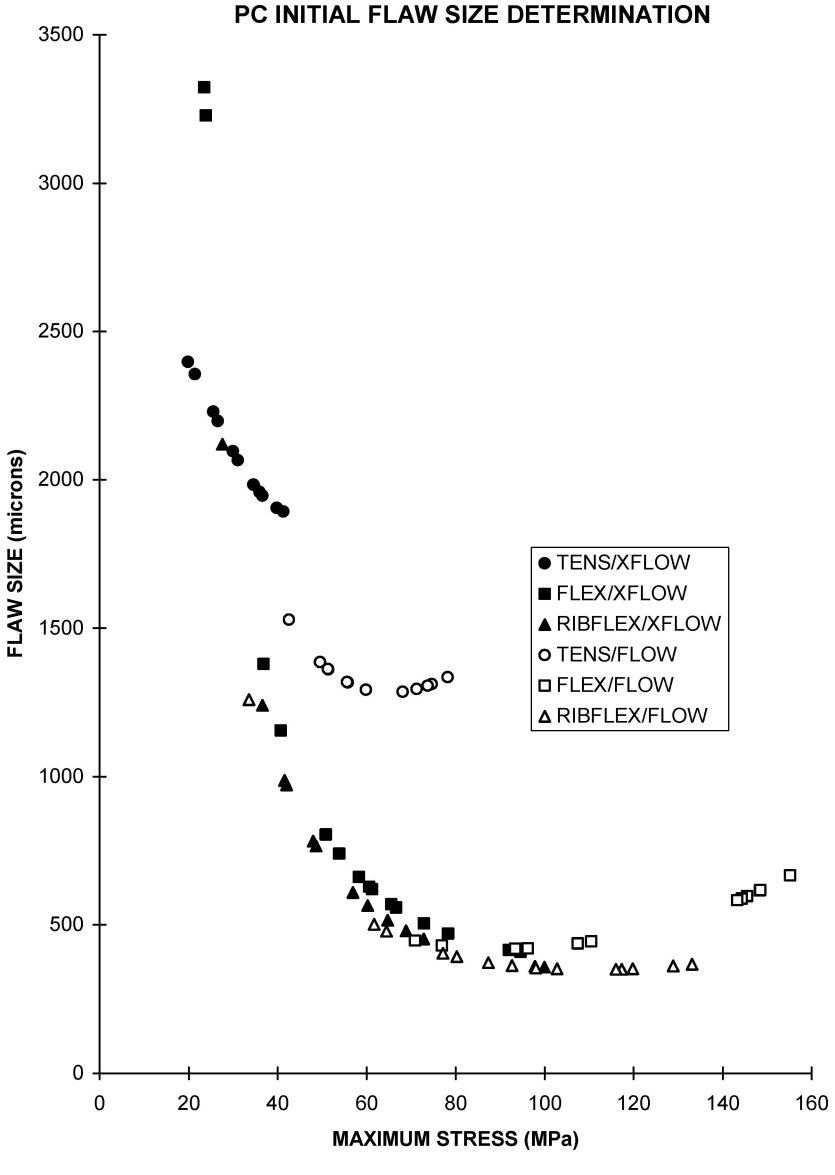

Figure 16 Initial flaw sizes for PC material calculated from various S-N datasets as indicated. See Reference 9 for details on S-N data.

S-N data for the flow direction can be predicted to be similar to the data for flat samples as it was observed to be. Predictions can also be made using the flaw sizes for geometries having different Y values, e.g., corner cracks or at holes. For the crossflow direction there is not a similar example since it is known that the fiber orientation in the crossflow rib is not similar to that in the flat area of the plaque. However the degree to which the use of a constant flaw size fits the corresponding crossflow data was shown, and, in spite of the larger variation in flaw size with stress level, the fit of the entire S-N curve is very good.

When combined with the strain energy release rate model and modulus data, the value of the fracture mechanics model predictions are amplified greatly. As was done here for the flow direction results, knowing the modulus allows us to predict the fatigue crack growth rate data, which in turn allows us to calculate corresponding S-N predictions. All that is required is the modulus change and in most cases the modulus can be accurately calculated for these fiber filled systems [6]. For example the effect of fiber concentration or use of different types of fibers can now be predicted. Other predictions, such as the influence of mean stress level or waveform will require first remeasuring the crack growth rate data under these specific conditions. Even so, the latter is very rapid compared to remeasuring an entire S-N curve. Although the flaw size itself is seen to depend on fiber orientation, the use of crossflow initial flaw sizes would appear to give conservative estimates for flow direction predictions.

This study has also shown some serious shortcomings of a simple fracture mechanics approach. With the single flaw size model it is not possible to obtain accurate S-N predictions for PBT, and for PC in the crossflow orientation. Also it is apparent that the exact procedure for measuring the fatigue crack growth rate is very important along with the fitting of the data to the Paris equation. One can argue that an initiation phase along with a propagation phase must somehow be included. The need for fatigue precracking in itself seems to be evidence that a mature damage zone is required at the crack tip to allow a fracture mechanics analysis to be employed. Similarly one might argue that the geometry factor, Y, is not properly represented since it is well known that Y should be a function of crack length. In

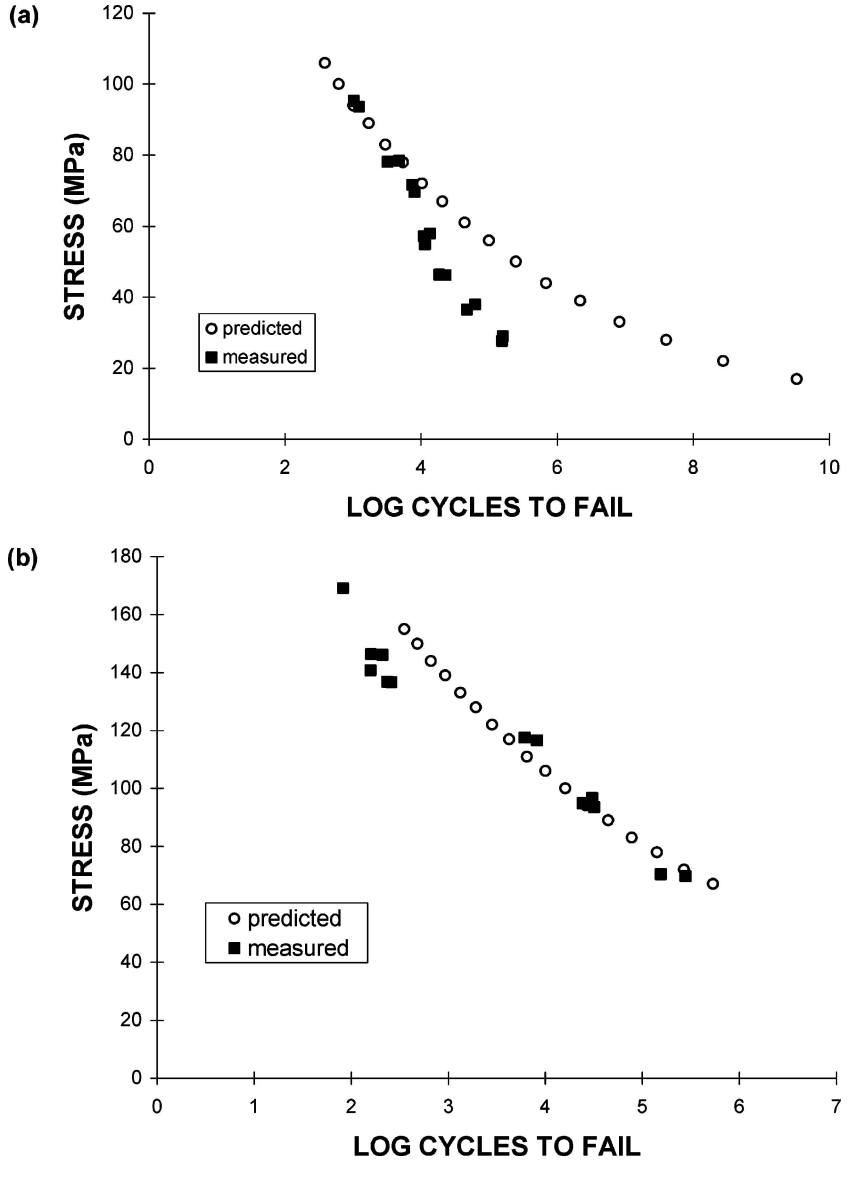

Figure 17 Comparison of predicted and measured S-N data for PC in the flexural fatigue test for the (a) Xflow and (b) Flow direction specimens.

this initial study, it was our intent to keep the model as simple as possible. We can surmise that a different initial flaw geometry or more complicated expression for Y might give improved results for the PBT and PC however attempts to modify these variables have not shown significant improvement in predictions for these cases. Another possibility is simply that the mechanism of fatigue failure for PA does primarily involve the growth of an existing flaw or precrack, whereas other mechanisms such as crack initiation or matrix yielding, are contributing more strongly to the fatigue fracture of PBT and PC.

As a final note, although it is tempting to give a physical explanation or significance to the calculated flaw sizes, it is clear from this preliminary investigation that many variables and assumptions are involved in the analysis. Therefore at this time the flaw sizes are considered only as mathematical fitting parameters without regard to their physical interpretation. Moreover, if tensile data rather than flexural data are used in deriving the initial flaw sizes, larger values are obtained. The tensile data are to be preferred for reasons previously stated [10] and this will be the subject of a subsequent publication involving a modified fracture mechanics approach.

6. Conclusions

Fatigue crack propagation rate data were obtained for the same three glass fiber reinforced plastics whose S-N behavior was previously determined. From the present analysis results it is concluded that:

1. Accurate S-N predictions are possible for some materials using a fracture mechanics model.
2. The best results are obtained for glass filled polyamide, (nylon 66) and polycarbonate, however, with polybutylene terephthalate, predictions were poor.
3. S-N data for other fiber orientations can be predicted from a single fatigue crack propagation rate measurement by using modulus changes and a strain energy release rate based fracture mechanics model to first predict crack growth rates for that orientation.
4. The initial flaw size depends on fiber orientation, with flaw sizes in the flow direction being about a factor of two lower than those in the Xflow direction.

Acknowledgement

The authors wish to thank Professor J. Gordon Williams of Imperial College for most helpful discussions concerning the application of fracture mechanics principles to reinforced thermoplastics.

References

1. N. E. DOWLING, "Mechanical Behavior of Materials" (Prentice Hall, 1993).
2. "SAE Fatigue Design Handbook," AE-10, 2nd ed., 1988.
3. R. W. HERTZBERG and J. A. MANSON, "Fatigue of Engineering Plastics" (Academic Press, 1980).
4. K. L. REIFSNIDER (ed.), "Fatigue of Composite Materials" (Elsevier, 1991).
5. D. C. MARTIN, G. E. NOVAK and M. G. WYZGOSKI, *J. Appl. Polym. Sci.* **37** (1989) 3029.
6. M. G. WYZGOSKI and G. E. NOVAK, *J. Mater. Sci.* **26** (1991) 6314.
7. M. G. WYZGOSKI, G. E. NOVAK and D. L. SIMON, *ibid.* **25** (1990) 4501.
8. A. PEGORETTI and T. RICCO, *Comp. Sci. Techn.* **59** (1999) 1055.
9. J. A. KROHN, G. E. NOVAK and M. G. WYZGOSKI, Paper # 455, Society of Plastics Engineers ANTEC 2001.
10. M. G. WYZGOSKI, J. A. KROHN and G. E. NOVAK, *Polym. Comp.*, submitted for publication, 2003.
11. A. J. KINLOCH and R. J. YOUNG, "Fracture Behavior of Polymers" (Applied Science, 1983).
12. J. G. WILLIAMS, "Fracture Mechanics of Polymers" (Ellis Norwood Lmt., 1984).
13. K. FRIEDRICH (ed.), "Composite Materials Series, 6: Application of Fracture Mechanics to Composite Materials" (Elsevier, 1989).
14. D. R. MOORE, A. PAVAN and J. G. WILLIAMS (eds.), ESIS Publication 28: "Fracture Mechanics Testing for Polymers, Adhesives and Composites" (Elsevier, 2001).
15. Y. MURAKAMI (ed.), "Stress Intensity Factors Handbook" (Pergamon Press, 1987).
16. Annual Book of ASTM Standards, Vol. 8.03, D5045-99, 331.
17. B. E. VER WEYST, C. L. TUCKER, P. H. FOSS and J. F. O'GARA, *Intern. Polym. Proc.* **14** (1999) 409.
18. M. G. WYZGOSKI and G. E. NOVAK, *Polym. Comp.* **16** (1995) 38.
19. M. G. WYZGOSKI and G. E. NOVAK, in "Ninth Intern. Conf., Deformation Yield and Fracture," (Cambridge, UK, 1994) p. 39/1.

Received 2 February
and accepted 31 August 2004